Depth profiling analysis of CuIn_{1-x}Ga_xSe₂ absorber layer by laser induced breakdown spectroscopy in atmospheric conditions

Chan Kyu Kim, Seok Hee Lee, Jung Hwan In, Hak Jae Lee, and Sungho Jeong*

School of Mechatronics, Gwangju Institute of Science and Technology, 1 Oryong-dong Buk- gu, Gwangju 500-712, South Korea

*shjeong@gist.ac.kr

Abstract: This work reports the capability of depth profile analysis of thin $CuIn_{1-x}Ga_xSe_2$ (CIGS) absorber layer (1.89 µm) with a sub-hundred nanometer resolution by laser induced breakdown spectroscopy (LIBS). The LIBS analysis was carried out with a commercial CIGS solar cell on flexible substrate by using a pulsed Nd:YAG laser ($\lambda = 532$ nm, $\tau = 5$ ns, top-hat profile) and an intensified charge-coupled device spectrometer in atmospheric conditions. The measured LIBS elemental profiles across the CIGS layer agreed closely to those measured by secondary ion mass spectrometry. The resolution of depth profile analysis was about 88 nm. Owing to the short measurement time of LIBS and the capability of in-air measurement, it is expected that LIBS can be applied for in situ analysis of elemental composition and their distribution across the film thickness during development and manufacturing of CIGS solar cells.

©2013 Optical Society of America

OCIS codes: (310.0310) Thin films; (350.6050) Solar energy; (300.6365) Spectroscopy, laser induced breakdown.

References and links

- National Renewable Energy Laboratory (NREL), Best Research-Cell Efficiencies, http://www.nrel.gov/ncpv/images/efficiency_chart.jpg, (updated at March, 2013).
- S. Niki, M. Contreras, I. Repins, M. Powalla, K. Kushiya, S. Ishizuka, and K. Matsubara, "CIGS absorbers and processes," Prog. Photovolt. Res. Appl. 18(6), 453–466 (2010).
- P. Jackson, D. Hariskos, E. Lotter, S. Paetel, W. Roland, R. Menner, W. Wischmann, and M. Powalla, "New world record efficiency for Cu(In, Ga)Se₂ thin-film solar cells beyond 20%," Prog. Photovolt. Res. Appl. 19(7), 894–897 (2011)
- J. T. Heath, J. D. Cohen, W. N. Shafarman, D. X. Liao, and A. A. Rockett, "Effect of Ga content on defect states in CuIn_{1-x}Ga_xSe₂ photovoltaic devices," Appl. Phys. Lett. 80(24), 4540–4542 (2002).
- O. Lundberg, M. Bodegård, J. Malmström, and L. Stolt, "Influence of the Cu(In, Ga)Se₂ thickness and Ga Grading on Solar Cell Performance," Prog. Photovolt. Res. Appl. 11, 77–88 (2003).
- S. M. Schleussner, T. Törndahl, M. Linnarsson, U. Zimmermann, T. Wätjen, and M. Edoff, "Development of gallium gradients in three-stage Cu(In, Ga)Se₂ co-evaporation processes," Prog. Photovolt. Res. Appl. 20(3), 284–293 (2012).
- M. A. Contreras, J. Tuttle, A. Gabor, A. Tennant, and K. Ramanathan, "High Efficiency Cu(in, Ga)Se₂-based solar cells: processing of novel absorber structures," in *Proceeding of IEEE Conference on First World Conference on Photovoltaic Energy Conversion* (IEEE, 1994), pp. 68–75.
- 8. J. H. Yoon, T. Y. Seong, and J. H. Jeong, "Effect of a Mo back contact on Na diffusion in CIGS thin film solar cells," Prog. Photovolt. Res. Appl. 21(1), 58–63 (2013).
- Y. Jeong, C. W. Kim, D. W. Park, S. C. Jung, J. Lee, and H. S. Shim, "Field modulation in Na-incorporated Cu(In,Ga)Se₂ (CIGS) polycrystalline films influenced by alloy-hardening and pair-annihilation probabilities," Nanoscale Res. Lett. 6(1), 581 (2011).
- S. Ishizuka, A. Yamada, M. M. Islam, H. Shibata, P. Fons, T. Sakurai, K. Akimoto, and S. Niki, "Na-induced variations in the structural, optical, and electrical properties of Cu(In, Ga)Se₂ thin film," J. Appl. Phys. 106(3), 034908 (2009).
- C. L. Perkins, B. Egaas, I. Repins, and B. To, "Quantitative analysis of graded Cu(In_{1-x}, Ga_x)Se₂ thin films by AES, ICP-OES, and EPMA," Appl. Surf. Sci. 257(3), 878–886 (2010).
- W. C. Lim, J. Lee, S. Won, and Y. Lee, "Characterization of Cu(In, Ga)Se₂ (CIGS) thin film in solar cell devices," Surf. Interface Anal. 44(6), 724–728 (2012).

- 13. M. M. Islam, T. Sakurai, A. Yamada, S. Otagiri, S. Ishizuka, K. Matsubara, S. Niki, and K. Akimoto, "Determination of Cu(In_{1-x}, Ga_x)₃Se₅ defect phase in MBE grown Cu(In_{1-x}Ga_x)Se₂ thin film by Rietveld analysis," Sol. Energy Mater. Sol. Cells 95(1), 231-234 (2011).
- 14. S. W. Schmitt, C. Venzago, B. Hoffmann, V. Sivakov, T. Hofmann, J. Michler, S. Christiansen, and G. Gamez, Glow discharge techniques in the chemical analysis of photovoltaic materials," Prog. Photovolt: Res. Appl. http://onlinelibrary.wiley.com/doi/10.1002/pip.2264/abstract (published on line).
- 15. K. Herz, A. Eicke, F. Kessler, R. Wächter, and M. Powalla, "Diffusion Barriers for CIGS solar cells on metallic substrates," Thin Solid Films 431-432, 392-397 (2003).
- D. W. Niles, K. Ramanathan, F. Hasoon, and R. Nouff, "Na impurity chemistry in photovoltaic CIGS thin films: Investigation with x-ray photoelectron spectroscopy," J. Vac. Sci. Technol. A 15(6), 3044–3049 (1997).
- 17. I. L. Eisgruber, B. Joshi, N. Gomez, J. Britt, and T. Vincent, "In situ X-ray fluorescence used for real-time control of CuIn_xGa_{1-x}Se₂ thin film composition," Thin Solid Films **408**(1-2), 64–72 (2002).

 18. S. H. Lee, H. S. Shim, C. K. Kim, J. H. Yoo, R. E. Russo, and S. Jeong, "Analysis of the absorption layer of
- CIGS solar cell by laser-induced breakdown spectroscopy," Appl. Opt. 51(7), B115-B120 (2012).
- J. H. In, C. K. Kim, S. H. Lee, and S. Jeong, "Reproducibility of CIGS thin film analysis by laser-induced breakdown spectroscopy," J. Anal. At. Spectrom. 28(4), 473-481 (2013).
- 20. J. H. In, C. K. Kim, S. H. Lee, H. S. Shim, and S. Jeong, "Quantitative analysis of CuIn_{1-x}Ga_xSe₂ thin films with fluctuation of operational parameters using laser-induced breakdown spectroscopy," J. Anal. At. Spectrom. **28**(6), 890–900 (2013).
- 21. S. Darwiche, M. Benmansour, N. Eliezer, and D. Morvan, "Laser-induced breakdown spectroscopy for photovoltaic silicon wafer analysis," Prog. Photovolt. Res. Appl. 20(4), 463-471 (2012).
- D. G. Papazoglou, V. Papadakis, and D. Anglos, "In situ interferometric depth and topography monitoring in LIBS elemental profiling of multi-layer structures," J. Anal. At. Spectrom. 19(4), 483-488 (2004).
- 23. J. M. Vadillo, C. C. Garcia, S. Palanco, and J. J. Laserna, "Nanometric range depth-resolved analysis of coatedsteels using laser-induced breakdown spectrometry with a 308 nm collimated beam," J. Anal. At. Spectrom. 13, 793-797 (1998).
- 24. M. P. Mateo, J. M. Vadillo, and J. J. Laserna, "Irradiance-dependent depth profiling of layered materials using laser-induced plasma spectrometry," J. Anal. At. Spectrom. 16(11), 1317–1321 (2001).
- 25. M. Abdelhamid, S. Grassini, E. Angelini, G. M. Ingo, and M. A. Harith, "Depth profiling of coated metallic artifacts adopting laser-induced breakdown spectrometry," Spectrochim. Acta, B At. Spectrosc. 65(8), 695-701
- 26. M. Milán, P. Lucena, L. M. Cabalín, and J. J. Laserna, "Depth profiling of phosphorus in photonic-grade silicon using laser-induced breakdown spectrometry," Appl. Spectrosc. 52(3), 444-448 (1998).
- 27. M. Hidalgo, F. Martín, and J. J. Laserna, "Laser-induced breakdown spectrometry of titanium dioxide antireflection coatings in photovoltaic cells," Anal. Chem. 68(7), 1095–1100 (1996).
- 28. S. H. Lee, C. K. Kim, J. H. In, D. S. Kim, H. J. Ham, and S. H. Jeong, "Nd:YAG laser ablation characteristics of thin CIGS solar cell films," Appl. Phys. B. in press., doi:10.1007/s00340-013-5477-3.
- Y. Ralchenko, A. E. Kramida, J. Reader, and NIST ASD Team (2008) "NIST Atomic Spectra Database, version 3.1.5 (National Institute of Standards and Technology, 2009)", http://physics.nist.gov/asd3.

1. Introduction

The performance of CuIn_{1-x}Ga_xSe₂ (CIGS) solar cell has been steadily improved in recent years and recorded a record high efficiency of 20.4% lately [1]. The achievement of high cell efficiency in CIGS solar cells is expected to allow the commercialization and mass production of CIGS thin film solar cells as the major photovoltaic products in the near future in place of crystalline silicon solar cells [2]. The efficiency of a CIGS solar cell is influenced by several factors such as elemental composition of the major constituent elements, elemental profile over the CIGS layer, Ga/(Ga + In) and Cu/(Ga + In) ratios, Na doping and grain size, etc [2–10]. Among the various factors that affect the efficiency of CIGS solar cells, elemental composition within the thin CIGS film and the profile of elemental concentration over the film thickness are crucial factors directly governing cell efficiency. For instance, the concentration ratio of Ga/(Ga + In) was known to influence the band gap of CIGS and a higher efficiency could be achieved when the Ga profile along film depth had a notch shape [5-7]. Also, it was reported that Na content strongly affected the solar cell efficiency because it controlled the grain size of CIGS [9,10]. Accordingly, an accurate control of the composition of constituent elements as well as their distribution within the CIGS thin film are critical to ensure the fabrication of high efficiency solar cell.

For the elemental analysis of CIGS thin films, various analytical methods have been employed in earlier studies such as Auger electron spectroscopy (AES) [4,11], inductively coupled plasma-optical emission spectrometry [5,11], wavelength-dispersed electron probe microanalysis [11-13], Glow discharge mass spectrometry (GD-MS) [14], secondary ion mass spectrometry (SIMS) [6,8-10,15], sputtered neutral mass spectrometry [15], x-ray photoelectron spectroscopy (XPS) [16], X-ray florescence (XRF) [3,17] or laser induced breakdown spectroscopy (LIBS) [18–20]. Among these analytical techniques, SIMS, GD-MS, AES and XPS have been successfully applied for the measurement of depth wise distribution of elements with high resolution [9-12,14,16]. However, since these methods for depth profile analysis required high vacuum for measurement, they were applicable only for the laboratory analysis of post-production CIGS samples but not suitable for in situ analysis. The capability of in situ analysis of the elemental composition and distribution would enable a real time verification of the composition change in CIGS layers during manufacturing processes, potentially saving significant cost by preventing production of defective products. To be applicable for in situ measurement at manufacturing sites, it is further required that the measurement can be performed in atmospheric conditions. Among the various methods, only XRF and LIBS measurements can be carried out in air [17-21]. Although the bulk composition of CIGS layers can be measured with XRF, it is difficult to implement XRF for depth profile analysis because the penetration depth of x-ray is much greater than the CIGS film thickness, approximately 50-300 µm for the x-ray photon energy range of 25-50 keV [19].

Alternatively, it has been shown that LIBS could be effectively applied for in situ monitoring of elemental composition at atmospheric conditions [21] with depth profiling capability [22–27]. LIBS measurement can be completed in less than one second. Also, provided that the concentration of a trace element varied with enough spatial resolution, LIBS has the potential to accurately measure the elemental profile along the depth of a solid [22–27]. For example, it was shown that the depth profile of phosphorus doped silicon could be analyzed with a resolution of a few micrometers [26]. The feasibility of depth profile analysis of titanium dioxide (TiO₂) antireflection coating on a silicon photovoltaic cell was also reported [27]. It was known that a collimated beam was more advantageous in improving resolution for depth profile analysis of metal [23]. Previously, we demonstrated the feasibility of depth profiling of CIGS films by LIBS in which it was shown that the variation of concentration ratios of constituent elements could be predicted with good accuracy with increasing shot number [19]. Although the possibility of depth profile analysis of CIGS thin films by LIBS has been suggested in our earlier study [18,19], a quantitative depth profiling analysis of CIGS solar cell films has not been reported yet.

In this work, we report the results for depth profile analysis of thin CIGS solar cell films by nanosecond laser based LIBS. It is demonstrated that the depth profile of constituent elements of CIGS absorber layer can be measured with a spatial resolution below 100 nm. The results showed that the depth profiles measured by LIBS and SIMS methods agreed closely.

2. Experiment

2.1 CIGS sample

A commercially available CIGS solar cell (10.4-12.7% aperture efficiency) was used as the sample for the depth profiling experiments in this study. The CIGS absorber layer of the sample was deposited on Mo-coated stainless steel foil by co-evaporation method. For LIBS measurement, first the protective cover layer of the CIGS solar cell was removed and then the sample was wet etched in a dilute hydrochloric acid and nitric acid solution for 2 min in order to remove the transparent conducting oxide (TCO) and the buffer layers. The bulk composition of the exposed CIGS layer was measured to be Cu 24.47 \pm 0.35, In 12.06 \pm 0.36, Ga 8.96 \pm 0.21, and Se 54.50 \pm 0.31 in atomic percent (at%) by XRF (Solar Metrology., SMX-BEN). The average thickness of the CIGS layer measured from the scanning electron microscope (SEM; Hitach, S-4800) image shown in Fig. 1(a) was 1.89 \pm 0.06 μm . The thickness of Mo layer measured from the SEM image was about 0.81 μm .

2.2 LIBS measurement

LIBS measurement of the CIGS layer was carried out using a commercial LIBS system (Applied Spectra Inc., RT250EC) with an intensified charge-coupled device (ICCD) spectrometer. The CIGS film was irradiated by a second harmonic Nd-YAG laser (λ = 532 nm, τ = 5 ns, multimode, top-hat profile) of the system with a laser spot diameter of about 200 µm at the sample surface. The 532 nm laser was selected because a strong surface absorption as in an opaque sample occurs at this wavelength due to its high photon energy (2.34eV) exceeding the band gap energy of CIGS (~1.0-1.7eV) [5, 28], an advantage for layer by by layer removal during depth profiling. The plasma emission was collected by a collection lens and delivered to the ICCD spectrometer via an optical fiber bundle. The schematic of the LIBS measurement set up is shown in Fig. 1(b). For depth profile analysis, LIBS spectra were collected from ten different spots on the CIGS sample. Each of the ten measurement spots were irradiated by thirty consecutive laser shots at the repetition rate of 1 Hz while collecting the LIBS spectra of each shot. The LIBS spectra at the same shot number from the ten measurement spots were then averaged to represent the LIBS intensity at the corresponding shot number and utilized for depth profiling analysis.

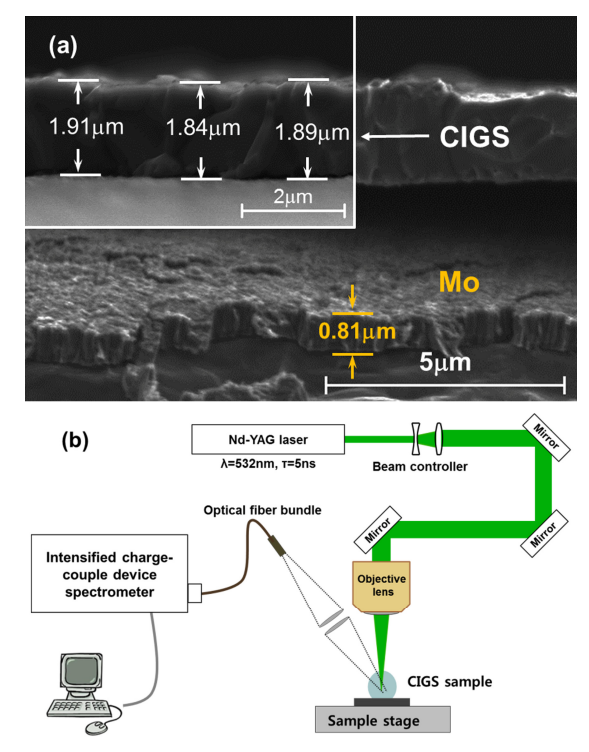


Fig. 1. (a) SEM image of the CIGS layer (TCO and buffer layers were removed) and (b) schematic diagram of the LIBS experiment set up.

2.3 SIMS measurement

For comparison with the LIBS measurement results, the profiles of constituent elements along the depth of CIGS sample were also measured by SIMS (Cameca, IMS-7f). The SIMS measurements were carried out using Cs⁺ as the primary ion with an acceleration voltage of 5 kV at an ultra-high vacuum condition (\sim 5 × 10⁻⁷ Pa). The depth profiles were obtained by raster scanning over a 170 × 170 μ m² area at the primary beam current of 50 nA. It took about 12 min until the CIGS layer was completely ablated by SIMS measurement.

3. Results and discussion

3.1 Determination of optimal measurement conditions

The ablation thickness of CIGS layer per pulse during LIBS measurement depends primarily on the laser pulse energy. To improve the spatial resolution of depth profiling, it is necessary to utilize the minimum pulse energy for ablation so that a layer by layer analysis of the film composition can be achieved with the possible highest resolution. Thus, an experiment was carried out to determine the minimum laser pulse energy for CIGS ablation but with sufficiently high plasma emission intensity for ICCD detection. The minimum laser pulse energy with sufficient signal to background ratio of the LIBS spectra was then determined to be 0.24 mJ (0.15 GW/cm²). At this laser pulse energy, the optimal delay of ICCD detector gating from the moment of laser firing (gate delay) was determined to be 0.2 μ s and the duration of gate opening for the collection of emission signal (gate width) to be 10 μ s. At these optimal detector conditions, the signal to background ratio of 4.19 was achieved for the spectral line of Ga(I) 417.204 nm. The gain of ICCD detector was set to 10 for the measurements.

Figure 2(a) shows the morphology of craters irradiated by different number of laser pulses (0.15 GW/cm²). The SEM images of the crater surface show that the CIGS layer was ablated nearly uniformly irrespective of laser pulse number. When the pulse number was increased close to 20, the CIGS layer was almost completely ablated and the underlying Mo layer started to appear in the middle of crater. For instance, energy dispersive x-ray spectroscopy

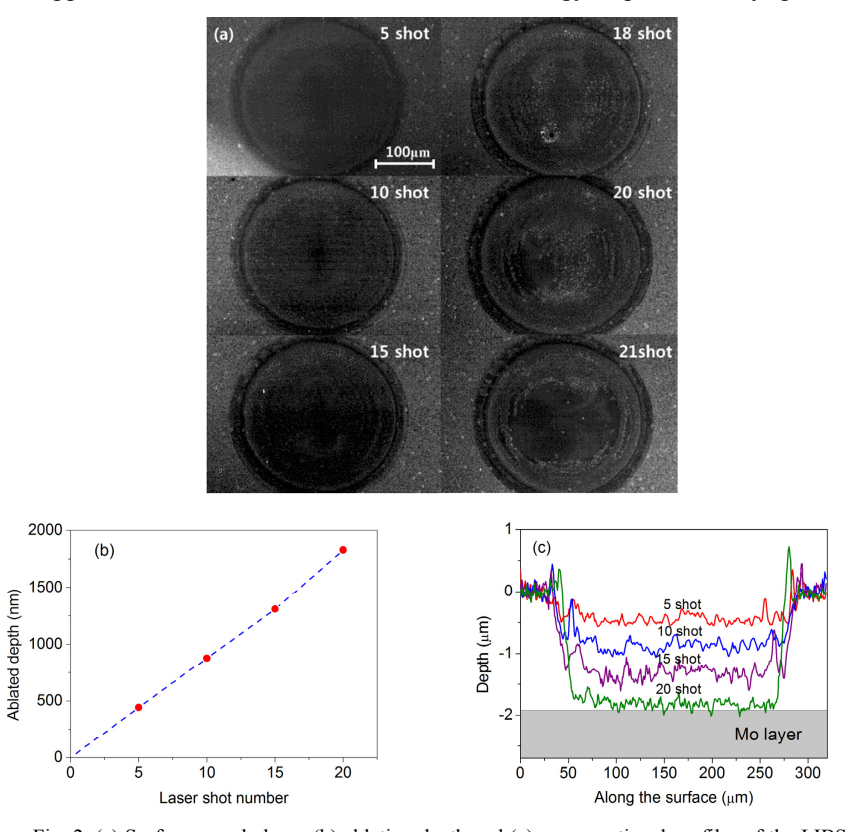


Fig. 2. (a) Surface morphology, (b) ablation depth and (c) cross-sectional profiles of the LIBS craters for varying laser shot number. (Laser irradiance: 0.15 GW/cm²).

(Horiba Ltd, EX250) measurement on the middle of the crater for pulse number 21 in Fig. 2(a) showed approximately 70% Mo and 25% Se, confirming the near complete ablation of CIGS layer.

As shown in Fig. 2(b), the average crater depth increased highly linearly with increasing pulse number for the ablation of CIGS layer. The average ablation rate per pulse of the CIGS layer up to the pulse number of 15 was about 88 nm. However, the average ablation rate increase slightly to 90.8 nm as the Mo layer started to appear as observed from the data between pulse numbers of 15 and 20 in Fig. 2(b). Figure 2(c) shows the cross-sectional profiles of the craters produced by varying number of pulses measured with a scanning confocal microscope (NanoFocus Inc.). The average roughness of the crater bottom surface slightly increased with increasing pulse number as summarized in Table 1. Compared to the roughness of the original CIGS surface (62nm), the change of surface roughness due to laser ablation is considered to be negligibly small. The linearity of ablation depth with respect to pulse number in Fig. 2(b) and the little change in surface roughness of the LIBS craters suggest that the layer-by-layer ablation of CIGS thin film can be done with high spatial resolution and accuracy. Note that when the Mo layer started to appear, the average roughness dropped significantly, possibly due to the elemental homogeneity of the Mo layer.

Table 1. Properties of LIBS craters for increasing laser shot number

Laser shot number	Ablation depth (nm)	Average ablation thickness per pulse (nm)	Average roughness (nm)
5	444.0	88.8	60.1
10	878.1	87.8	68.2
15	1307.8	87.5	77.5
20	1829.0	90.8	53.5

For comparison, the morphology and cross-sectional profile of the CIGS thin film during SIMS measurement are also shown in Figs. 3(a) and 3(b), respectively. The SIMS crater also showed uniform surface morphology with a slightly rounded bottom surface. The average surface roughness of the SIMS crater at the intermediate depth of 0.65 μ m was about 61 nm, equal to that of the original CIGS surface.

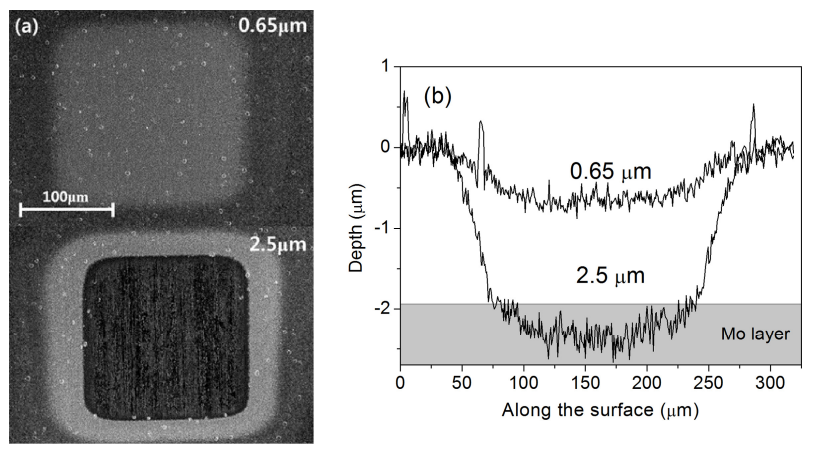


Fig. 3. (a) Surface morphology and (b) cross-sectional profiles of the SIMS craters.

3.2 Depth profile analysis

Figure 4 shows the averaged LIBS spectra from the ten measurement spots of the CIGS sample; the first shot from each of the ten spots was utilized for averaging. The analysis of Se was excluded in the present study because Se emission lines were observed only in the ultraviolet regime and their intensities were too weak to be clearly measured at the low laser

energy condition of present experiments. The spectral information of the Cu(I), Ga(I), In(I) and Na(I) emission lines in Fig. 4 is listed in Table 2 [29]. The intensities of measured LIBS spectra were normalized by the total spectral area to obtain normalized LIBS signal intensities since the absolute intensity of each element varied. The relative standard deviation (RSD) of the normalized intensities of each element from the ten spots was below 15%.

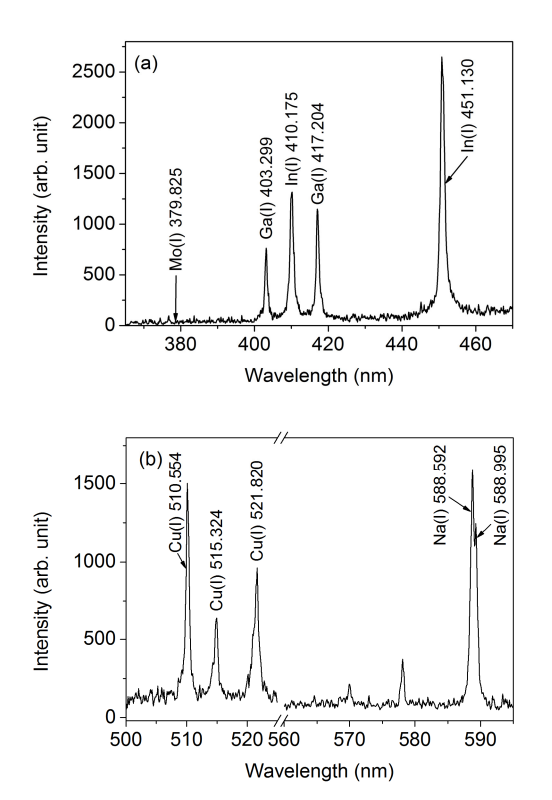


Fig. 4. Typical LIBS spectra of the CIGS layer in spectral regions of (a) 375-470nm and (b) 500-600nm (gate delay: 0.2μs, gate width: 10μs).

Table 2. Spectral characteristics of Ga, In, Cu and Na emission lines. (λ_{ij} : transition wavelength, A_{ij} : transition probability, E_i and E_j : upper and lower energy levels, and g_i - g_i : degeneracy of upper and lower energy state)^a

Element	λ _{ij} (nm)	\mathbf{g}_{i} - \mathbf{g}_{j}	$A_{ij} (10^8 s^{-1})$	$E_i - E_j (eV)$
Ga(I)	403.299	2-2	0.485	0.0000 - 3.0734
Ga (I)	417.204	4-2	0.945	0.1024 - 3.0734
In (I)	410.175	2-2	0.560	0.0000 - 3.0218
In (I)	451.130	4-2	1.020	0.2743 - 3.0218
Cu (I)	510.554	6-4	0.020	1.3889 - 3.8167
Cu (I)	515.324	2-4	0.600	3.7859 - 6.1912
Cu (I)	521.820	4-6	0.750	3.8167 - 6.1912
Na (I)	588.995	2-4	0.616	0.0000 - 2.1044
Na (I)	588.592	2-2	0.614	0.0000 - 2.1023
From [29]				

Figure 5 shows the intensity correlation plots of Ga(I) 417.204 nm - Ga(I) 403.299 nm and In(I) 410.175 nm - In(I) 451.130 nm line pairs of the CIGS LIBS spectra measured from 300 laser shots (10 spots \times 30 shots per spot). The intensities of the two Ga or In emission lines show an excellent linear correlation; $I_{Ga(I)417.204} = 0.543 \times I_{Ga(I)403.299}$ and $I_{In(I)451.130} = 2.497 \times I_{In(I)410.175}$. Since the two Ga or In emission lines have a linear correlation, the sum of their normalized intensities was used as the Ga or In intensity for the depth profile analysis in

this study. The use of summation intensity instead of single peak intensity reduced the relative standard deviation (RSD), especially at depths where the signal intensity was weak. Similarly, the intensity of Na emission line was also represented by the sum of intensities of the two overlaid Na lines (Na(I) 588.995 nm and Na(I) 588.592 nm) in Fig. 4. On the other hand, Cu(I) 510.554 nm was selected for Cu intensity because the intensity of Cu(I) 515.324 nm and Cu(I) 521.820 nm emission lines became weaker or disappeared at times as the pulse number was increased.

Figures 6(a) and 6(b) show the depth profiles of the constituent elements of CIGS layer measured by LIBS and SIMS methods, respectively, with respect to ablated film depths. For

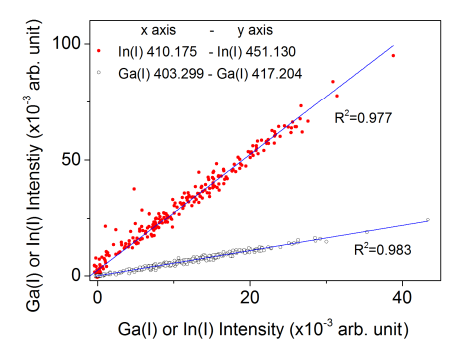


Fig. 5. Intensity correlation of the Ga and In line pairs used for summation intensity calculation.

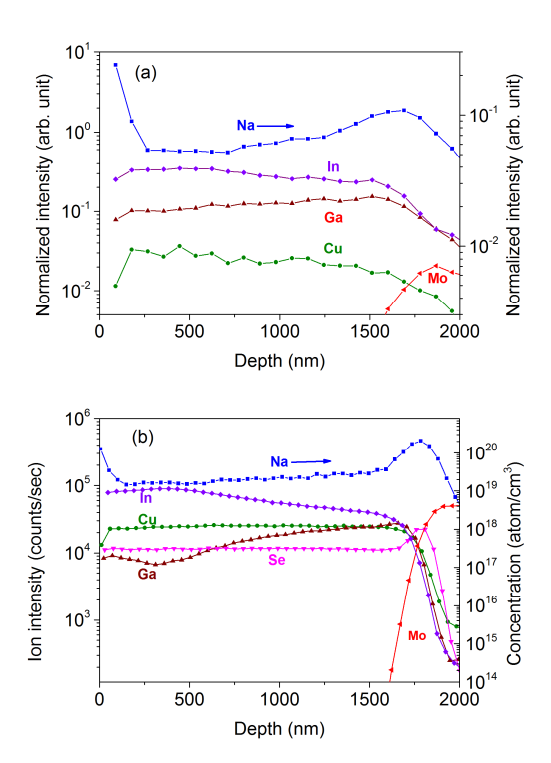


Fig. 6. Depth profiles of the CIGS absorber layer measured by (a) LIBS and (b) SIMS. The LIBS intensity profile of Na was independently scaled for clear comparison with the SIMS data

the LIBS data in Fig. 6(a), the film depth was obtained by converting the pulse number into depth by multiplying the average ablation thickness per pulse (88.0 nm). For the SIMS data in Fig. 6(b), the film depth was estimated by multiplying the measurement time by the average sputtering rate of CIGS (2.63 nm/s). Comparison of the depth profiles generated by LIBS in Fig. 6(a) and those by SIMS in Fig. 6(b) shows that the depth profiles of Ga, In, Na, and Mo measured by LIBS and SIMS agree closely. The closeness of these profiles is understood to imply that an accurate depth profile analysis of CIGS layer may be possible by LIBS. Note that due to the difference in the measurement methods only the shape of depth profiles or the tendency of intensity changes of each element in Fig. 6 is meaningful to compare.

Based on the LIBS and SIMS data in Fig. 6, the depth profiles of Ga/In ratio and Na were examined in further detail as follow. The Ga/In ratio is a parameter that governs band gap of CIGS and needs to be strictly controlled to ensure high cell efficiency [5–7] and Na is also known to strongly influence the efficiency of CIGS solar cells [9,10]. Figure 7 shows the profiles of Ga/In ratio along the depth of CIGS layer measured by both LIBS and SIMS. These profiles show almost identical shapes; an initial shallow bump up to about 300 nm depth, a broadly increasing Ga/In ratio up to about 1600 nm, and a final sharp peak centered at around 1800 nm with rapid drop. These results verify that the depth profile of CIGS thin films can be analyzed by LIBS to the accuracy level almost equivalent to that could be achieved by SIMS.

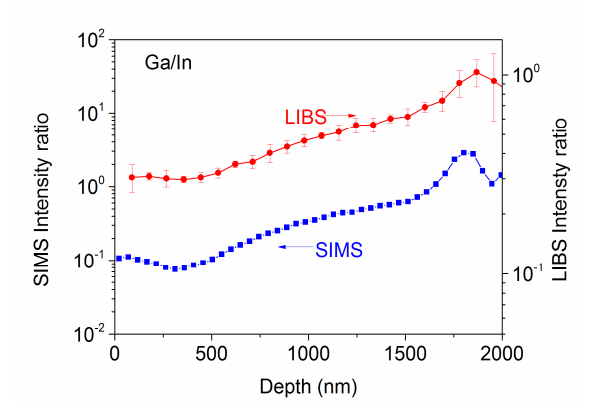


Fig. 7. Comparison of the Ga/In intensity ratios predicted by LIBS and SIMS with respect to film depth.

Note that the SIMS system utilized in the present study was calibrated using a standard material (Evans Analysis Group) to predict the absolute Na concentration from the measured SIMS signal intensity. Using the Na concentration of the CIGS sample predicted by SIMS measurement as the reference data, the LIBS signal intensity of Na was recalibrated for absolute concentration. Since the number of data points between each LIBS and SIMS measurement were different, the concentration data predicted by SIMS within the resolution of LIBS (~88 nm) were averaged for the calibration of LIBS signal intensity. As shown in Fig. 8(a), a good linear correlation crossing the origin was observed between the normalized LIBS Na intensity and the Na concentration (atom/cm³) predicted by SIMS measurement. When the measured LIBS Na intensity was converted to concentration using the calibration curve in Fig. 8(a) and plotted with the concentration predicted by SIMS measurement, they agreed closely as shown in Fig. 8(b).

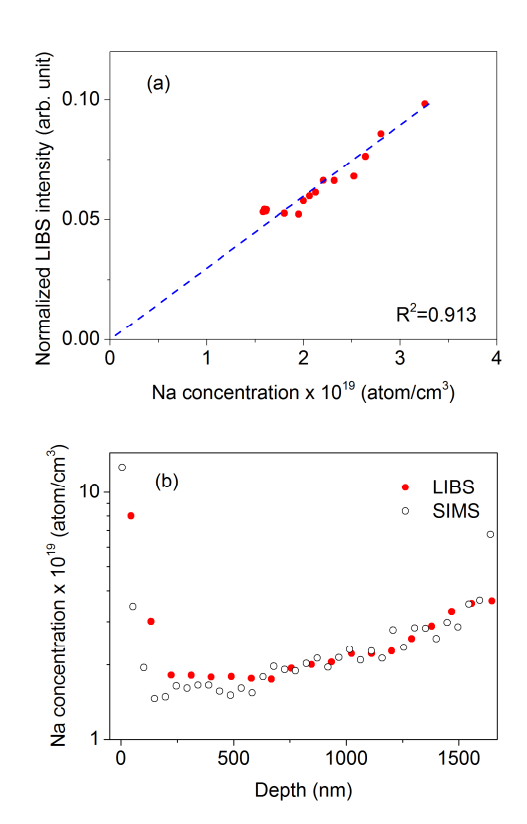


Fig. 8. (a) Calibration curve of the LIBS Na intensity and (b) the Na profiles predicted by LIBS and SIMS.

4. Conclusion

In this work, we demonstrated that the depth profile of major constituent elements of CIGS absorber layer can be analyzed with high accuracy and resolution by LIBS. The results suggest that LIBS can provide a powerful method for in situ depth profiling analysis when incorporated with its intrinsic short measurement time and capability of in-air measurement. The real time verification of the composition and depth profiles of CIGS absorber layer by LIBS can be effectively applied for the characterization of CIGS layer during solar cell development and for the quality control of products during manufacturing.

Acknowledgment

This work was supported by the National Research Foundation of Korea (NRF) grant funded by the Korea government (MEST) (No. 2013-064113).